THERMAL EFFECT ON MASS FLOW-RATE OF SONIC NOZZLE

by

Hong-Bing DING, Chao WANG*, and Gang WANG

Tianjin Key Laboratory of Process Measurement and Control,
School of Electrical Engineering and Automation,
Tianjin University, Tianjin, China

Original scientific paper
https://doi.org/10.2298/TSCI151104146D

Sonic nozzles are widely used as flow measurement and transfer standard. The thermal effect of sonic nozzle is significant at low Reynolds number. It includes two correction factors, C_T for the thermal boundary-layer and C_α for constrained thermal deformation of throat area. Firstly, using the similarity solution, the formula for correction factor C_T over wall temperature range from $0.8T_0$ to $1.2T_0$ was obtained. For $\gamma = 1.33$, $C_T = 1 - 3.800\ Re^{-1/2}\Delta T/T_0$; for $\gamma = 1.4$, $C_T = 1 - 3.845\ Re^{-1/2}\Delta T/T_0$; for $\gamma = 1.67$, $C_T = 1 - 4.010\ Re^{-1/2}\Delta T/T_0$. Secondly, thermal and stress models for partially constrained expansion were built. Unlike the free expansion, truth slopes of C_α for three nozzles are $+1.74\cdot10^{-6}$, $-2.75\cdot10^{-5}$ and $-3.61\cdot10^{-5}$, respectively. Lastly, the experimental data of Cu nozzle was used to validate present results. It revealed that modified experimental values are in good agreement with the present result.

Key words: *sonic nozzle, thermal effect, thermal boundary-layer, constrained thermal deformation*

Introduction

Background

Sonic nozzles are applied in accuracy measurement and control of gas-flow due to its stability, simple structure, and good repeatability. Over 70% sonic nozzles were used as a standard gas meters to calibrate other types meters [1]. Under critical flow condition, real mass flow-rate of sonic nozzle is calculated by [2]:

$$q_m = C_\mathrm{d} q_{mi} = \frac{C_\mathrm{d} C_* A_\mathrm{nt} p_0}{\sqrt{\mathrm{R_m} T_0}} \tag{1}$$

where C_d is the discharge coefficient for adiabatic wall, C_* – the critical flow factor, $A_\mathrm{nt} = \pi d^2/4$, $\mathrm{R_m} = R/\mathrm{M}$, p_0 and T_0 are inlet stagnation pressure and temperature, respectively.

The gas expands and accelerates in sonic nozzle and its temperature will drop greatly. Then, the nozzle body will be cooled by forced convection heat transfer between the wall surface and the fluid [3]. Subsequently, thermal boundary-layer and throat area will be changed which is called *thermal effect*. The thermal effect is significant at low Reynolds number [4]. For the last decade, thermal effect of sonic nozzle had been investigated by Bignell and Choi [5], Li and Mickan [6], Hu *et al.* [7], Wright *et al.* [3], and Unsal *et al.* [4].

* Corresponding author, e-mail: wangchao@tju.edu.cn

Considering thermal effect, mass flow rate eq. (1) is rewritten:

$$q_{m,T_\mathrm{w}} = [C_\mathrm{d} + (C_T - 1)]\frac{C_*(C_\alpha A_\mathrm{nt})p_0}{\sqrt{R_\mathrm{m}T_0}} \tag{2}$$

where C_T is the correction factor for the thermal boundary-layer, $C_\alpha = A/A_\mathrm{ref}$ – the correction factor for the thermal deformation of the throat area.

Thermal boundary-layer

During the last few decades, many investigators, such as, Illingworth [8], Li and Nagamatsu [9], Cohen and Reshotko [10], Ball [11], Back [12], Aziz [13], and Kendoush [14], made a great deal of researches about the effect of wall temperature on laminar boundary-layer. For the compressible flow, Illingworth [8], and Li and Nagamatsu [9] put forward similarity methods for calculating the properties of laminar compressible boundary-layer in an axial pressure gradient with heat transfer. However, the results are only suitable for planar flow and the main-stream velocities must satisfy special-relationship which differs from flow characteristic of sonic nozzle. Subsequently, Cohen and Reshotko [10], and Ball [11] presented an approximate method for the calculation of the compressible laminar boundary-layer with heat transfer and arbitrary pressure gradient, based on Stewartson's transformation and Thwaites' correlation concept. Back [12] proposed a similarity solution of the laminar boundary-layer equation for a large range of flow acceleration, surface cooling, and flow speeds in supersonic nozzle. However, in their works, the target variable is local Reynolds number, Re_x, rather than throat Reynolds number. These results can not be directly applicable to flow meter.

For mass flow-rate of sonic nozzle, Tang [15], Geropp [16], and Ishibashi and Takamoto [17] presented the analytical similarity solutions of boundary-layer of sonic nozzle by some remarkable and praiseworthy transforms. Unfortunately, their models based on adiabatic wall boundary were not able to analyze the thermal effect on mass flow rate of sonic nozzle. Johnson *et al.* [18] presented CFD results showing a decrease in discharge coefficient for a nozzle warmer than the adiabatic body temperature due to a thermal boundary-layer and pointed out that the magnitude of the thermal boundary-layer effect is proportional to $\mathrm{Re}^{-1/2}$ and specific heat ratio, γ.

Thermal expansion of the nozzle throat area

For the thermal expansion on material, it is necessary to consider whether the body is free to expand or is constrained. If the body is free to expand, the thermal deformation or strain is simply calculated by the thermal expansion coefficient which produces no stress. If the body is partially constrained, then internal stress and thermal deformation is more complicated [19]. Thomas *et al.* [20] and Park *et al.* [21] analyzed the thermal and mechanical behavior of constrained copper molds. The comparison of stress-total strain between unconstrained and practical constrained conditions was obtained. Cragun and Howell [22] presented the constrained thermal expansion micro-actuator. Isfahani *et al.* [23] simulated thermal stress and cooling deformations of the mold which is constrained by the die. Ansola *et al.* [24] mentioned Chevron and Guckel micro-actuators will deform and produce lateral bending due to constrained thermal expansion. In 2013, Stavely [25] investigated the deformation occurs in contact-aided compliant mechanisms with temperature change. The results indicated that the constrained displacement is normal to the structural connection joint. All researches can help us understand thermal effect on sonic nozzle.

Present work

In this study, the following specific tasks were made.

– To obtain correction factor, C_T, for the thermal boundary-layer.
– A similarity solution for its thermal boundary-layer with wall heat transfer was presented. By definition of C_T, its formula was obtained.
– To obtain correction factor C_α for constrained thermal deformation of throat area.

The thermal and stress models for partially constrained expansion were built. Thermal stress and deformation were illustrated to analyze the process of partially constrained expansion. The truth formula of C_α for different nozzles were obtained. Lastly, the experimental data of Cu nozzle was used to validate the formula. After modified, the experiments agreed well with present formula.

Similarity solution for C_T

Similarity equations and reducibility

For a curvilinear system of co-ordinates, fig. 1, x is wall surface and y is the co-ordinate at perpendicular angle to the surface. The body radii $r_\mathrm{w}(x)$ is perpendicular to axis. The velocity components parallel and normal to the wall will be denoted by u and v, respectively. The continuity, momentum and energy equations of compressible laminar boundary-layer are expressed as [26]:

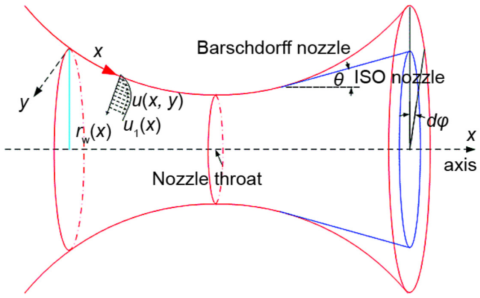

Figure 1. Sonic nozzles and curvilinear system of co-ordinates

$$\begin{cases} \dfrac{\partial(\rho u r_\mathrm{w}^s)}{\partial x} + \dfrac{\partial(\rho v r_\mathrm{w}^s)}{\partial y} = 0 \\ \rho\left(u\dfrac{\partial u}{\partial x} + v\dfrac{\partial u}{\partial y}\right) = -\dfrac{\partial p}{\partial x} + \dfrac{\partial}{\partial y}\left(\mu\dfrac{\partial u}{\partial y}\right), \quad 0 = \dfrac{\partial p}{\partial y} \\ \rho\left[u\dfrac{\partial(c_p T)}{\partial x} + v\dfrac{\partial(c_p T)}{\partial y}\right] = u\dfrac{\partial p}{\partial x} + \mu\left(\dfrac{\partial u}{\partial y}\right)^2 + \dfrac{\partial}{\partial y}\left(k\dfrac{\partial T}{\partial y}\right) \end{cases} \tag{3}$$

where $s = 0$ for planar and $s = 1$ for axisymmetric.

It is assumed the fluid is perfect gas. Additionally, the effect of viscosity and heat conduction in the main-stream of nozzle can be neglected. Further assume that:

$$\mu = \frac{\mu_0}{T_0}T \tag{4}$$

$$\mathrm{Pr} = 1 \Rightarrow \quad k = \mu c_p = c_p\frac{\mu_0}{T_0}T \tag{5}$$

In order to reduce PDE (3) to ODE, we define stream function ψ as:

$$\psi(x,y)=\int_0^y \frac{u(x,y)}{T(x,y)}\,\mathrm{d}y \tag{6}$$

and introduce a co-ordinate transformation:

$$\eta=\int_0^y \frac{u_1(x)}{N(x)T(x,y)}\,\mathrm{d}y \tag{7}$$

Then, further assume that:

$$\psi(x,y)=N(x)K(\eta) \tag{8}$$

$$u(x,y)=u_1(x)F(\eta) \tag{9}$$

$$e(x,y)=e_1(x)G(\eta) \tag{10}$$

where η is the similar variable. $K(\eta)$, $F(\eta)$, and $G(\eta)$ are dimensionless stream function, velocity, and total energy, respectively.

Combining eqs. (6), (8), and (9), we get:

$$\frac{\partial\eta}{\partial y}=\frac{u_1F}{TNK'} \tag{11}$$

where $K'=\mathrm{d}/\mathrm{d}\eta$. Compared with eq. (7), it is implied that $F=K'$.

Next, some assumptions should be put forward to reduce boundary-layer equations to ODE. Because Geropp's assumption is not suitable to non-adiabatic wall, the follow equations were introduced:

$$\frac{c_p}{\mathrm{R_m}T_1}\frac{\mathrm{d}T_1}{\mathrm{d}x}+\frac{1}{r_\mathrm{w}^s}\frac{\mathrm{d}r_\mathrm{w}^s}{\mathrm{d}x}+\frac{1}{N}\frac{\mathrm{d}N}{\mathrm{d}x}=m\frac{1}{u_1}\frac{\mathrm{d}u_1}{\mathrm{d}x}\left(1+\frac{\gamma-1}{2}\mathrm{M}_1^2\right) \tag{12}$$

$$\frac{\mathrm{R_m}\mu_0}{T_0}\frac{u_1}{N^2p_1}=m\frac{1}{u_1}\frac{\mathrm{d}u_1}{\mathrm{d}x}\left(1+\frac{\gamma-1}{2}\mathrm{M}_1^2\right) \tag{13}$$

where $\eta(x, y)$ is derived in *Appendix A.1*. The nozzle parameter m is a function of nozzle geometry and isentropic exponent which is derived in *Appendix A.2*.

Finally, the boundary-layer equations can be rewritten as:

$$KK''+K'''=\frac{1}{m}(K'^2-G) \tag{14}$$

$$G''+KG'=0 \tag{15}$$

where the boundary conditions are:

$$\eta=0:\quad K=K'=0,\quad G=G_\mathrm{w}=\frac{T_\mathrm{w}}{T_0} \tag{16}$$

$$\eta=\infty,\quad K'=1,\quad G=1 \tag{17}$$

where it is assumed that $\eta=0$ or ∞ when $y=0$ or ∞, respectively.

Next, to thermal effect on its mass flow rate, the thermal boundary-layer profiles and displacement thickness were investigated in detail.

Boundary-layer profiles

A study of the similarity solution of boundary-layer can provide the understanding of the effect of wall heat transfer. Taking $R = 2d$ and $\gamma = 1.4$ as an example, we get $m = 0.4823$. Using eqs. (14)-(17), similarity solutions of K' and G for $m = 0.4823$ and different T_w/T_0 were plotted in fig. 2, where the expression $T_w/T_0 \to 0$ means T_w tends to absolute zero.

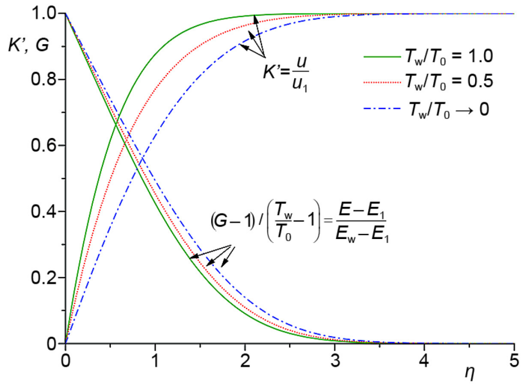

Figure 2. The similarity solutions of K' and G for $m = 0.4823$ ($R = 2d$ and $\gamma = 1.4$) and different T_w/T_0

Besides, it is found that:

$$\frac{T}{T_1} = G + \frac{\dfrac{\gamma-1}{\gamma+1}\lambda_1^2}{1-\dfrac{\gamma-1}{\gamma+1}\lambda_1^2}(G-K'^2) \tag{18}$$

Hence, the dimensionless mass flux, J, at the throat is calculated by:

$$J = \frac{u\rho}{u_1\rho_1} = \frac{\dfrac{u}{u_1}}{\dfrac{T}{T_1}} = \frac{K'}{G + \dfrac{\gamma-1}{2}(G-K'^2)} \tag{19}$$

The similarity solutions of T/T_1 and J at nozzle throat are shown in figs. 3 and 4.

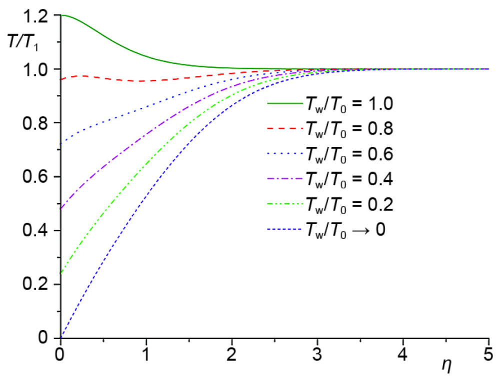

Figure 3. Similarity solutions of T/T_1 for $m = 0.4823$ ($R = 2d$ and $\gamma = 1.4$) and different T_w/T_0 at throat

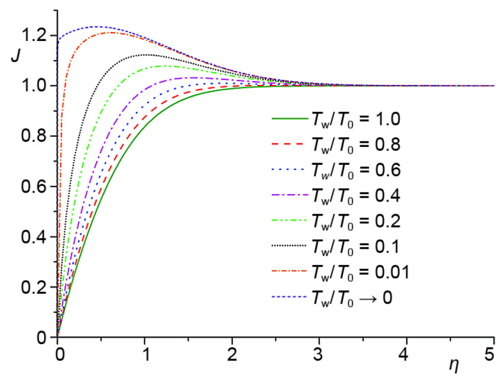

Figure 4. Similarity solutions of J for $m = 0.4823$ ($R = 2d$ and $\gamma = 1.4$) and different T_w/T_0 at throat

According to figs. 2 and 3, it is found that the dimensionless parameters $u(x, y)/u_1(x)$ and $T(x, y)/T_1(x)$ at the throat will drop with the decrease of T_w/T_0.

Additionally, eq. (19) shows that mass flux $J(x, y)$ is proportional to u/u_1 and inversely proportional to T/T_1. As shown in figs. 2 and 3, the decline rate of T/T_1 is larger than that of u/u_1. Hence, $J(x, y)$ at nozzle throat will gradually rise with the decrease of T_w/T_0, as shown in fig. 4.

Correction factor C_T

According to eq. (A.8), we get:

$$\mathrm{d}y = N_0 c_1^{\frac{m-(m+2)\gamma}{\gamma-1}} u_1^{m-1} \left(\frac{r_w}{r_{nt}}\right)^{-s} T\mathrm{d}\eta \tag{20}$$

Hence, the displacement thickness δ_1 of boundary-layer is calculated by:

$$\delta_1 = \int_0^\delta \left(1-\frac{\rho}{\rho_1}\frac{u}{u_1}\right)\mathrm{d}y = \int_0^\delta \left(1-\frac{T_1}{T}\frac{u}{u_1}\right)\mathrm{d}y = \int_0^\delta (1-J)\,\mathrm{d}y =$$

$$= N_0 \lambda_1^{\frac{s}{2}} \left(\frac{\gamma+1}{2}\right)^{\frac{s}{2(\gamma-1)}} \left(1-\frac{\gamma-1}{\gamma+1}\lambda_1^2\right)^{\frac{s}{2(\gamma-1)}} c_1^{\frac{m-(m+2)\gamma}{\gamma-1}} u_1^{m-1} T_1 \int_0^\infty \left(\frac{T}{T_1}-\frac{u}{u_1}\right)\mathrm{d}\eta \tag{21}$$

Substituting eqs. (A.6) and (18) into eq. (21), gives:

$$\frac{\delta_1}{d} = \frac{\left(\frac{\gamma+1}{2}\right)^{-\frac{1-s}{2(\gamma-1)}-\frac{m}{2}}}{\sqrt{\mathrm{Re}}\,\lambda_1^{1-\frac{s}{2}-m}\left(1-\frac{\gamma-1}{\gamma+1}\lambda_1^2\right)^{\frac{1-\frac{1}{2}s}{\gamma-1}+\frac{m}{2}}} \int_0^\infty \left[G+\frac{\frac{\gamma-1}{\gamma+1}\lambda_1^2}{1-\frac{\gamma-1}{\gamma+1}\lambda_1^2}(G-K'^2)-K'\right]\mathrm{d}\eta \tag{22}$$

where the throat Reynolds number Re $=\rho_{cr} c_{cr} d/\mu_0$.

At the throat, eq. (22) is reduced to:

$$\frac{\delta_1}{d} = \frac{\left(\frac{\gamma+1}{2}\right)^{\frac{1}{2(\gamma-1)}}}{\sqrt{\mathrm{Re}}} \int_0^\infty \left[G+\frac{\gamma-1}{2}(G-K'^2)-K'\right]\mathrm{d}\eta \tag{23}$$

The distributions of displacement thickness of sonic nozzle for various T_w/T_0 and γ are shown in figs. 5 and 6, where, $X = 0$ at the throat.

Figures 5 and 6 show that the displacement thickness δ_1 becomes thicker with the increase of γ and T_w/T_0, and the decrease of throat Reynolds number. Additionally, eq. (21) deduces that $\delta_1 = \int_0^\delta (1-J)\mathrm{d}y$, and fig. 4 shows that all values of mass flux J are greater than 1 when T_w/T_0 tends to 0. Thus, δ_1 is below 0 while T_w/T_0 tends to zero which means the actual flow-rate for non-adiabatic wall is larger than ideal flow-rate for adiabatic wall.

For adiabatic wall, discharge coefficient, C_d, is divided into three parts [27], namely viscous discharge coefficient, C_{d1}, affected by gas viscosity, inviscid discharge coefficient, C_{d2}, induced by multi-dimensional flow [28], and virial discharge coefficient, C_{d3}, affected by physical properties of real gas. Because C_{d3} could be negligible when the gas pressure is low, the discharge coefficient C_d just considers first two items and is described by [29]:

$$C_d = \frac{q_m}{q_{mi}} = C_{d1}C_{d2} = C_{d2}\left(1 - \frac{4\delta_{1,\mathrm{nt}}}{d}\right) \tag{24}$$

where $\delta_{1,\mathrm{nt}}$ the displacement thickness at nozzle throat.

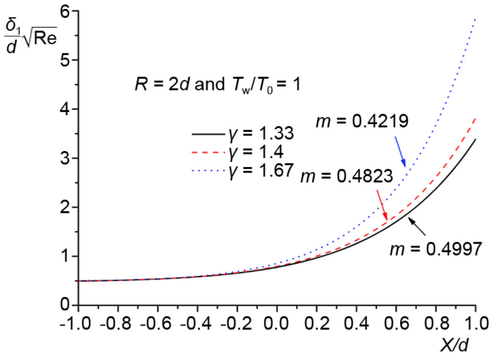

Figure 5. Distributions of displacement thickness of Barschdorff nozzle for $R = 2d$, $T_w/T_0 = 1$ and different γ

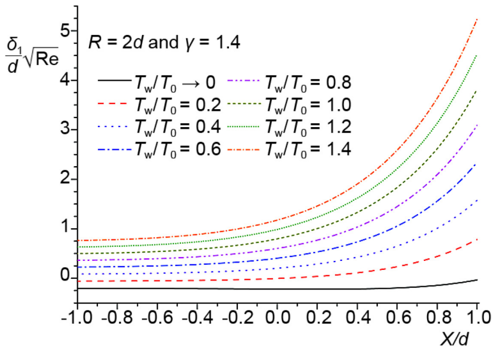

Figure 6. The distributions of displacement thickness of Barschdorff nozzle for $R = 2d$, $\gamma = 1.4$, and different T_w/T_0 (where $X = 0$ at the throat)

,Besides, according to Hall's theory [28], C_{d2} can be calculated by:

$$C_{d2} = 1 - \frac{\gamma+1}{\left(2\frac{R}{d}\right)^2}\left[\frac{1}{96} - \frac{8\gamma+21}{4608\left(2\frac{R}{d}\right)} + \frac{754\gamma^2+1971\gamma+2007}{552960\left(2\frac{R}{d}\right)^2}\right] \tag{25}$$

For $R = 2d$ and $\gamma = 1.4$. The C_{d2} remains constant 0.99859. Combining eq. (23), the discharge coefficient at $T_w = T_0$ is expressed as eq. (26) which is basically accord with empirical equation (accuracy: 0.2%) of ISO 9300 [2]. By definition, the correction factor $C_T \equiv 1$ for adiabatic wall:

$$C_d = 0.99859 - 3.181\,\mathrm{Re}^{-0.5} \tag{26}$$

For non-adiabatic wall, using the similarity solution, the correction factor C_T can be approximate to eq. (27) over the wall temperature range from $0.8T_0$ to $1.2T_0$:

$$C_T = \begin{cases} 1 - 3.800\,\mathrm{Re}^{-0.5}\dfrac{\Delta T}{T_0} & \text{for} \quad \gamma = 1.33 \\ 1 - 3.845\,\mathrm{Re}^{-0.5}\dfrac{\Delta T}{T_0} & \text{for} \quad \gamma = 1.4 \\ 1 - 4.010\,\mathrm{Re}^{-0.5}\dfrac{\Delta T}{T_0} & \textit{for} \quad \gamma = 1.67 \end{cases} \tag{27}$$

where ΔT is equal to $T_w - T_0$.

Next, CFD simulations are conducted to compare with eq. (27) by similarity solution. The experimental validation will be presented after investigating the characteristic of thermal deformation.

Software FLUENT is used to simulate the flow. The axisymmetric swirl laminar model and structured quad-map mesh are adopted [30, 31]. Discretization of the governing equations employs second-order upwind scheme, and the solution is obtained by a density-based approach. Fluid is perfect gas. The thermal conductivity and dynamic viscosity are function of local temperature. The throat Reynolds number is proportional to inlet pressure. Inlet and outlet boundary conditions are both pressure. The back pressure ratio is fixed at 0.1 to ensure to avoid the shock at the divergent section. The inlet stagnation temperature T_0 is fixed at 300 K. The wall temperature T_w = 285, 290, 295, 300, and 305 K. A grid size of 100 × 300 was performed to guarantee a grid independent solution.

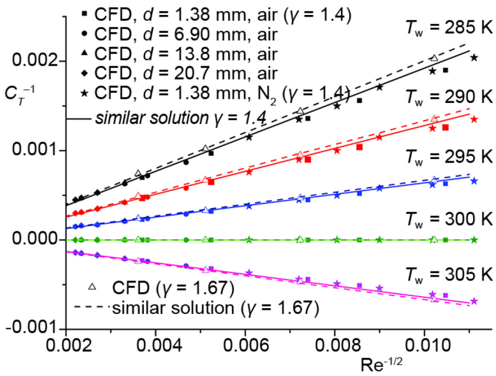

Figure 7. Comparison of C_T between eq. (27) and CFD for T_0 = 300 K and various γ, T_w

All results are shown in fig. 7. The stagnation (reference) temperature T_0 remains constant 300 K. The fluids include air (γ = 1.4), nitrogen (γ= 1.4), and argon (γ= 1.67). It is obvious that eq. (27) agrees well with simulate.

Partially constrained thermal expansion for C_α

Nozzle geometry, fixture, and loads

Three sonic nozzles reported by Wright *et al.* [3] were used to analyse the thermal deformation of nozzle throat. As is shown in fig. 8, the nozzle throat diameters at the reference temperature 298 K are 3.2 mm, 1.1 mm, and 0.65 mm, respectively. The material of nozzle is Cu whose thermal conductivity is 380 W/mK. A sheathed platinum resistance thermometer (RTD) was used as a PID controlled heater to maintain the CFV at the desired T_w set point values of 298 K, 303 K, 308 K, and 313 K.

Firstly, the geometry of nozzle body is plotted in fig. 8(b). These nozzles have the same external profile, thus the small diameter nozzle has the larger wall thickness.

Secondly, each nozzle was installed between inlet and outlet pipes made of fiberglass filled PTFE with O-ring seals, as shown in fig. 8(a). The PTFE material reduced conductive heat transfer between the heated nozzle body and the stainless steel pipe. The thermal conductivity of PTFE is 0.26 W/mK which is about 1/1400$^{\text{th}}$ that of Cu. It means that the temperatures of PTEE and pipeline are almost unaffected by heated nozzle. Besides, the left and right edges of nozzle body on O-ring seals are constrained to have no displacement in axis direction (x-direction).

Lastly, the body temperature distribution is nearly uniform and equal to the external controlled temperature, since the thermal conductivity of Cu is 380 W/mK and the Biot number is lower. Thus, thermal loads are that body temperatures set to a constant prescribed temperature.

Thermal and stress models

The governing equations and boundary conditions controlling the performance of thermal and structure of nozzle body were described.

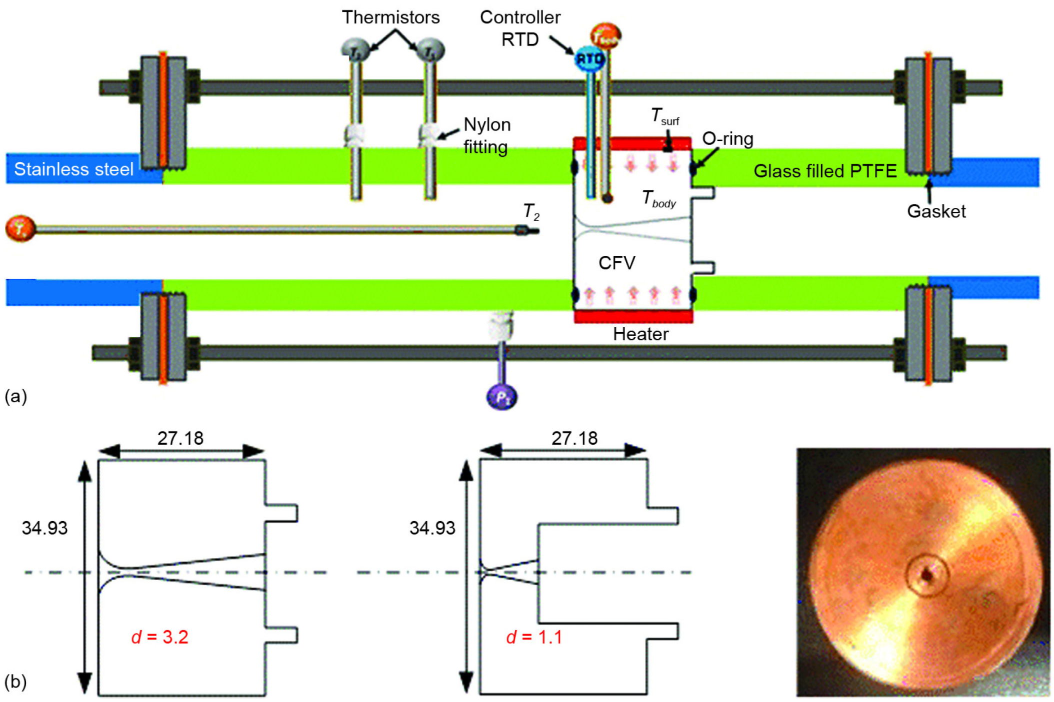

Figure 8. Experiment details reported by Wright *et al.* [3]; (a) experimental arrangement, (b) the geometry of sonic nozzle

It is assumed that the material of nozzle body has constant thermal conductivity, since the body temperature range is relatively small. The transient equilibrium equation without internal heat resource can be written:

$$\nabla^2 T_\mathrm{w} - \frac{1}{a^2}\frac{\partial T_\mathrm{w}}{\partial t} = 0 \tag{28}$$

where thermal diffusivity $a^2 = k/(\rho c_p)$. In this study, the body temperature is nearly uniform and steady, hence eq. (28) is reduced to $T_\mathrm{w} \equiv$ const.

Then, it is assumed the thermal deformation is small and reversible, and the elastic behavior is linear where the strain is proportional to the stress. Besides, the irreversible plastic and creep deformations were not considered. Hence, the constitutive equation for a linear isotropic thermo-elastic continuum is [32]:

$$\varepsilon_{ij} = \frac{1+\upsilon}{E}\sigma_{ij} - \left[\frac{\upsilon}{E}\sigma_{ii} - \alpha(T_\mathrm{w} - T_\mathrm{ref})\right]\delta_{i,j} \tag{29}$$

where ε and σ are strain and stress.

The boundary conditions in accordance with boundary loads in fig. 8 are applied to the element nodes:

Mechanical

- Nodes on O-ring seals of left and right edges are constrained to have no displacement in the X-direction.
- Nodes on other surfaces are un-constrained.

Thermal

– All nodes have the same temperature T_w.
– No internal heat is generated.

Thermal deformation and correction factor C_α

If the nozzle body is allowed to expand freely, the thermal deformation of the radius of flow channel is $\delta_r/r_w = \alpha\,\Delta T$. Thus, $C_\alpha = A/A_{ref} = 1 + 2\alpha\,\Delta T$. However, the results will be different when some parts or edges are constrained.

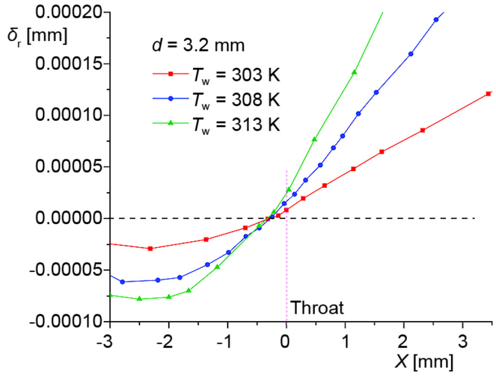

Figure 10. The radius variations of flow channel for 3.2 mm nozzle

Next, the partially constrained thermal deformation of nozzle body was investigated in detail. For Cu, Young's modulus and yield strength are $1.1\cdot10^{11}$ Pa and $2.75\cdot10^{8}$ Pa. Thermal conductivity k = 380 W/mK, thermal expansion coefficient $\alpha = 1.7\cdot10^{-5}$ and Poisson's ratio $\upsilon = 0.3$. Besides, the reference temperature $T_{ref} = T_0 = 298$ K.

For 3.2 mm nozzle, the predicted evolution of thermal deformation at 313 K (ΔT = 15 K) are shown in fig. 9. In case of free body thermal expansion, if the material is allowed to expand or contract freely, there are no stresses in the body. However, for partially constrained expansion, the deformation and stress become more complicated. fig. 9(a) shows thermal stress in *X-Y* plane is not equal to zero. The maximum of thermal stress is near the O-ring seals (constrained part) and is about $8.0\cdot10^{7}$ Pa which is less than yield strength of Cu. Thus, the irreversible plastic and creep deformations do not exist. fig. 9(b) illustrates that *Y*-displacement in *X-Y* plane is obviously different from free expansion.

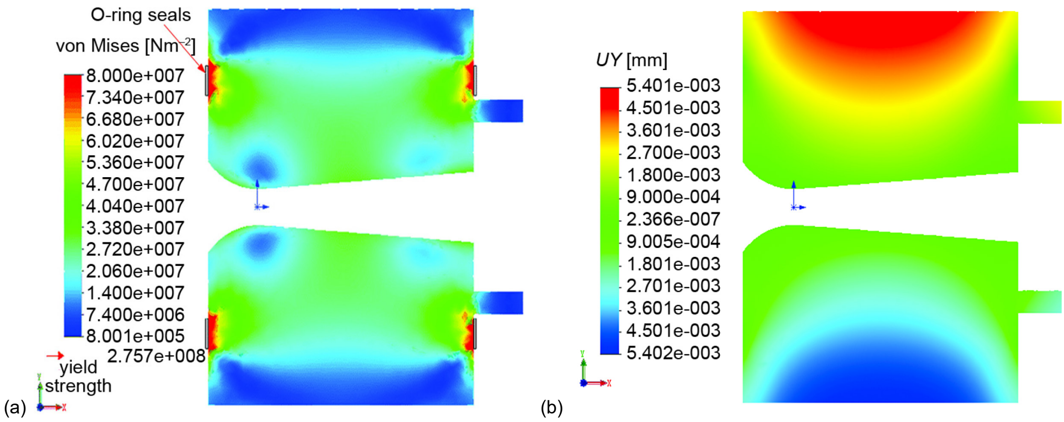

Figure 9. Predicted evolution of thermal deformation at 313 K for 3.2 mm nozzle; (a) thermal stress in *X-Y* plane, (b) *Y*-displacement in *X-Y* plane (*for color image see journal web site*)

The radius variations δ_r of flow channel for 3.2 mm nozzle are shown in fig. 10 and tab. 1. At ΔT = 15 K, for free expansion, δ_r is always greater than 0 and for constrained expansion, δ_r near the entrance is negative. Besides, although δ_r is positive at throat, its value $+2.1\cdot10^{-5}$ mm is less than $+4.08\cdot10^{-4}$ mm of free expansion.

For 1.1 mm nozzle, the thermal stress and deformation at 313 K (ΔT = 15 K) are plotted in fig. 11. Similarly, the thermal stress in this case is not equal to zero. The maximum of thermal stress is also less than yield strength of Cu. The radius variations δ_r for 1.1 mm nozzle are shown in fig. 12 and tab. 1. At ΔT = 15 K, δ_r upstream of throat is always negative. δ_r at the throat is –$1.13 \cdot 10^{-4}$ mm is significant less than $+1.40 \cdot 10^{-4}$ mm of free expansion. It means that the difference between constrained and unconstrained expansions gets bigger with the decrease of throat diameter. This might be because the small diameter nozzle has the larger wall thickness.

Table 1. Thermal deformation of constrained thermal expansion ($T_0 = T_{ref}$ = 298 K)

Throat Diameter, d	Body temperature T_w	Radius changes δ_r at the throat	$\delta A(T_w)/A(T_{ref})$	C_α
3.2 mm	313 K	$2.1 \cdot 10^{-5}$ mm	$2.63 \cdot 10^{-5}$	$C_\alpha = 1 + 1.74 \cdot 10^{-6} \Delta T$
	308 K	$1.4 \cdot 10^{-5}$ mm	$1.75 \cdot 10^{-5}$	
	303 K	$6.6 \cdot 10^{-6}$ mm	$8.25 \cdot 10^{-6}$	
1.1 mm	313 K	$-1.13 \cdot 10^{-4}$ mm	$-4.11 \cdot 10^{-4}$	$C_\alpha = 1 - 2.75 \cdot 10^{-5} \Delta T$
	308 K	$-7.65 \cdot 10^{-5}$ mm	$-2.78 \cdot 10^{-4}$	
	303 K	$-3.66 \cdot 10^{-5}$ mm	$-1.33 \cdot 10^{-4}$	
0.56 mm	313 K	$-7.58 \cdot 10^{-5}$ mm	$-5.42 \cdot 10^{-4}$	$C_\alpha = 1 - 3.61 \cdot 10^{-5} \Delta T$
	308 K	$-5.08 \cdot 10^{-5}$ mm	$-3.63 \cdot 10^{-4}$	
	303 K	$-2.45 \cdot 10^{-5}$ mm	$-1.75 \cdot 10^{-4}$	

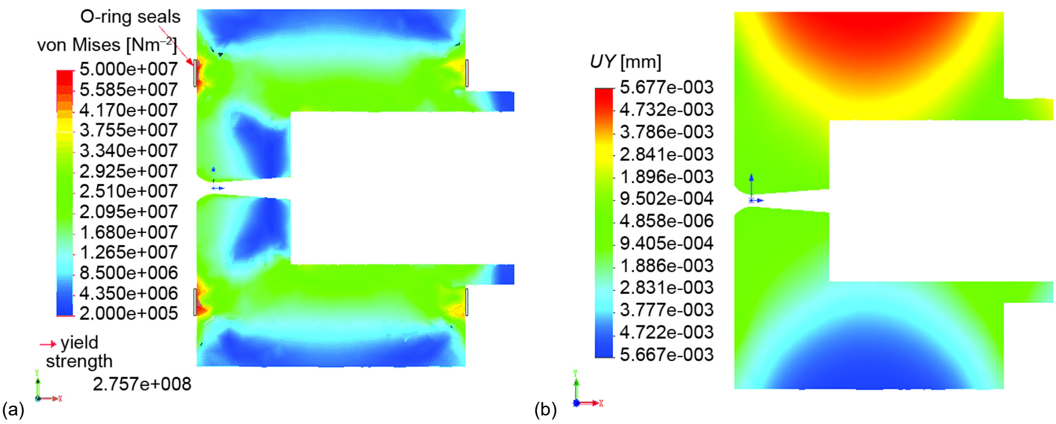

Figure 11. Predicted evolution of thermal deformation at 313 K for 1.1 mm nozzle; (a) thermal stress in *X-Y* plane, (b) *Y*-displacement in *X-Y* plane (*for color image see journal web site*)

Besides, figs. 10 and 12 also shows the radius changes for 1.1 mm nozzle at different ΔT = 15, 10, and 5 K. The results show the δ_r at different temperatures have a same tendency and its magnitude increases with the increase of ΔT.

Table 1 lists the results of correction factor C_α. The slopes of C_α for 3.2 mm, 1.1 mm, and 0.56 mm nozzles are $+1.74 \cdot 10^{-6}$, $-2.75 \cdot 10^{-5}$, and $-3.61 \cdot 10^{-5}$, respectively, while the slopes of C_α is a constant $+3.40 \cdot 10^{-5}$ for free expansion.

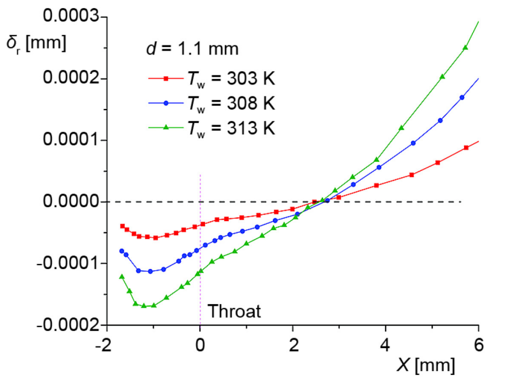

Figure 12. The radius changes of flow channel for 1.1 mm nozzle

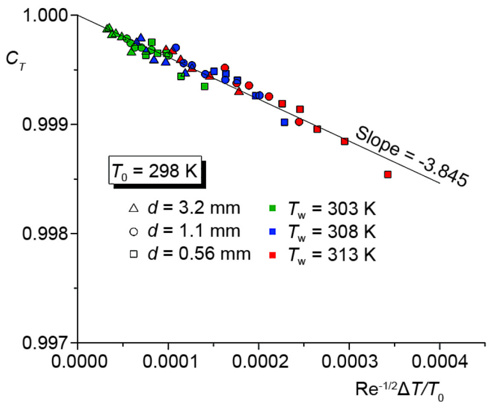

Figure 13. The C_T *vs.* $\mathrm{Re}^{-1/2}\Delta T/T_0$ for Cu nozzle, comparing the similarity solutions with experimental data by Wright *et al.* [3]

Experimental validation

The experimental data of Cu nozzle by Wright *et al.* [3] was used to validate the results of this study. The inlet stagnant temperature of dry air is approximate to 298 K. Each nozzles was calibrated with dry air at six pressure setpoints (100~700 kPa). The uncertainty of mass flow rate is about 0.06%.

For dry air, the slope of C_T of Wright *et al.* [3] and eq. (27) of this work are –7.05 and –3.845, respectively. The reason for this discrepancy was found out. In Wright's study, the simple correction factor $C_\alpha = 1 + 2\alpha\,\Delta T$ for free expansion was used directly whose slope is greater than truth value. Hence, by definition of eq. (2), the calculated slopes of C_T will be less than truth value.

Now, the truth values of C_α in tab. 1 for different nozzles were used to calculate new modified experimental values of C_T. The results are plotted in fig. 13. It reveals that the experimental values of C_T are in good agreement with eq. (27).

Conclusion

To study thermal effect on mass flow rate of sonic nozzle, both correction factor C_T for the thermal boundary-layer and correction factor C_α for constrained thermal deformation of the throat area were proposed. The results are outlined as follows.

- A similarity solution for its thermal boundary-layer with wall heat transfer was presented.
- For non-adiabatic wall, the formula for correction factor C_T over the wall temperature range from $0.8T_0$ to $1.2T_0$ was obtained. For $\gamma = 1.33$, $C_T = 1 - 3.800\mathrm{Re}^{-1/2}\Delta T/T_0$; for $\gamma = 1.4$, $C_T = 1 - 3.845\mathrm{Re}^{-1/2}\Delta T/T_0$; for $\gamma = 1.67$, $C_T = 1 - 4.010\mathrm{Re}^{-1/2}\Delta T/T_0$.
- Thermal and stress models for partially constrained thermal expansion of nozzle body were built.
- The truth slopes of C_α for 3.2 mm, 1.1 mm, and 0.56 mm nozzles are $+1.74\cdot10^{-6}$, $-2.75\cdot10^{-5}$ and $-3.61\cdot10^{-5}$, respectively, which are different from a constant value of free expansion $+3.40\cdot10^{-5}$.
- The experimental data of Cu nozzle was used to validate the results of this study. It showed that modified experimental values of C_T are in good agreement with eq. (27).

Acknowledgment

This work is supported by National Natural Science Foundation of China under Grant No. 51506148, Natural Science Foundation of Tianjin under Grant 16JCQNJC03700 and No. 15JCYBJC19200, Research Fund of Tianjin Key Laboratory of Process Measurement and Control under Grant No. TKLPMC-201611, and Program for New Century Excellent Talents in University under Grant No. NCET-10-0621.

Nomenclature

A – area, [m^2]
a – thermal diffusivity, $a^2 = k/(\rho c_p)$, [m^{2}s^{-1}]
c_p – isobaric heat capacity, [Jkg^{-1}K^{-1}]
C_d – discharge coefficient for the adiabatic wall, [–]
C_T, C_α – correction factor, [–]
C_* – critical flow factor, [–]
c – sound speed, [ms^{-1}]
d – throat diameter of nozzle, [mm]
E – Young's/elastic modulus, [Pa]
e – total energy ($c_pT + u^2/2$), [Jkg^{-1}]
F, G, K, N – defined in eqs. (8)-(10), [–]
J – dimensionless mass flux, [–]
k – thermal conductivity, [Wm^{-1}K^{-1}]
m – the nozzle parameter in eq. (12)
M – Mach number, [–]
N_0 – integration constant, [–]
Pr – Prandtl number, [–]
p – pressure, [Pa]
q_m, $q_{m\mathrm{i}}$ – real/ideal mass flow-rate, [kgs^{-1}]
R – radius of curvature, [m]
Re$_x$ – local Reynolds number ($= \rho_1 u_1 x/\mu_0$), [–]
Re – throat Reynolds number ($= \rho_{cr} c_{cr} d/\mu_0$), [–]
R$_\mathrm{m}$ – specific gas constant, [Jkg^{-1}K^{-1}]
s – for plannar = 0; for axisimetric = 1
T – temperature, [K]
ΔT – temperature difference ($=T_\mathrm{w} - T_0$), [K]
t – time, [s]
u, v – velocity in the x-, y-directions, [ms^{-1}]
X, Y, Z – Cartesian co-ordinates, [m]
x, y, r_w – curvilinear system of co-ordinates, [m]

Greek symbols

α – thermal expansion coefficient, [K^{-1}]
γ – isentropic exponent, [–]
δ_1 – displacement thickness, [mm]
$\delta_{\mathrm{i},j}$ – Kronecker's delta, [–]
δ_r – radius change of flow channel, [mm]
ε – strain, [–]
η – similar variable, [–]
θ – diffuser angle, [°]
λ – dimensionless velocity, [–]
μ – dynamic viscosity, [Pa·s]
ν – kinematic viscosity, [m^{2}s^{-1}]
ρ – density, [kgm^{-3}]
σ – stress, [Pa]
υ – Poisson's ratio, [–]
ψ – stream function, [m^{2}s^{-1}K^{-1}]

Subscripts

0 – at stagnation condition
1 – main-stream
cr – critical point
nt – at nozzle throat
ref – reference temperature
w – nozzle body

Appendix

A.1 Sufficient condition of reducibility to ODE

Equation (12) can be transformed into:

$$\frac{1}{N}\frac{\mathrm{d}N}{\mathrm{d}x} = \frac{m}{u_1}\frac{\mathrm{d}u_1}{\mathrm{d}x} - \frac{(m+2)\gamma - m}{\gamma - 1}\frac{1}{c_1}\frac{\mathrm{d}c_1}{\mathrm{d}x} - \frac{1}{r_\mathrm{w}^s}\frac{\mathrm{d}r_\mathrm{w}^s}{\mathrm{d}x} \tag{A.30}$$

Integrating eq. (A.1), we get:

$$N = N_0 u_1^m c_1^{\frac{m-(m+2)\gamma}{\gamma-1}} \left(\frac{r_\mathrm{w}}{r_\mathrm{nt}}\right)^{-s} \tag{A.31}$$

where N_0 is an integration constant. Li and Nagamatsu [9] directly assumed that $N_0^2 = R\mu_0/T_0$. However, for sonic nozzle, eq. (13) is rewritten:

$$\left(1+\frac{\gamma-1}{2}M_1^2\right)u_1^{2m-2}(c_1^2)^{\frac{m-(m+2)\gamma}{\gamma-1}}\left(\frac{r_\mathrm{w}}{r_\mathrm{nt}}\right)^{-2s}\frac{\mathrm{d}u_1}{\mathrm{d}x}=\frac{\mu_0}{m\frac{\rho_1}{\rho_0}\frac{T_1}{T_0}\rho_0T_0^2}\frac{1}{N_0^2} \tag{A.32}$$

Eq. (A.3) is reduced to:

$$\left(1-\frac{\gamma-1}{\gamma+1}\lambda_1^2\right)^{\frac{m+1-(m+2)\gamma}{\gamma-1}}\lambda_1^{2m-2}\left(\frac{r_\mathrm{w}}{r_\mathrm{nt}}\right)^{-2s}\mathrm{d}\lambda_1=\left(\frac{\gamma+1}{2}\right)^m\sqrt{\frac{2}{\gamma+1}}\frac{\nu_0}{mT_0^2N_0^2}c_0^{\frac{5\gamma-1}{\gamma-1}}\mathrm{d}x \tag{A.33}$$

Let:

$$d=\frac{T_0^2N_0^2}{\nu_0c_0^{(5\gamma-1)/(\gamma-1)}}\sqrt{\frac{\gamma+1}{2}} \tag{A.34}$$

where d is throat diameter. Thus, integration constant N_0 can be expressed:

$$N_0=\frac{\left[\nu_0c_0^{(5\gamma-1)/(\gamma-1)}d\sqrt{\frac{2}{\gamma+1}}\right]^{0,5}}{T_0} \tag{A.35}$$

At the moment, eq. (A.4) is transformed into:

$$\int_{\lambda_s}^{\lambda_1}m\left(\frac{2}{\gamma+1}\right)^m\left(1-\frac{\gamma-1}{\gamma+1}\lambda_1^2\right)^{\frac{m+1-(m+2)\gamma}{\gamma-1}}\lambda_1^{2m-2}\left(\frac{r_\mathrm{w}}{r_\mathrm{nt}}\right)^{-2s}\mathrm{d}\lambda=\frac{x}{d} \tag{A.36}$$

Besides, according to eq. (7) and eq. (A.2), $\eta(x, y)$ is expressed:

$$\eta(x,y)=\frac{1}{N_0}\int_0^y c_1^{\frac{\gamma(m+2)-m}{\gamma-1}}u_1^{1-m}\left(\frac{r_\mathrm{w}}{r_\mathrm{nt}}\right)^s\frac{\mathrm{d}y}{T(x,y)} \tag{A.37}$$

A.2 The parameter m for the nozzle flow

To solve the boundary-layer of sonic nozzle, the value of parameter m for the nozzle should be determined. Assuming the main-stream flow is 1-D isentropic, the cross-section area can be calculated by [33]:

$$\left(\frac{r_\mathrm{w}}{r_\mathrm{nt}}\right)^{s+1}=\frac{1}{\lambda_1\left(\frac{\gamma+1}{2}\right)^{\frac{1}{\gamma-1}}\left(1-\frac{\gamma-1}{\gamma+1}\lambda_1^2\right)^{\frac{1}{\gamma-1}}} \tag{A.38}$$

Substituting eq. (A.9) into eq. (A.7), gives:

$$\int_{\lambda_a}^{\lambda_1}m\left(\frac{2}{\gamma+1}\right)^{m-\frac{s}{\gamma-1}}\left(1-\frac{\gamma-1}{\gamma+1}\lambda_1^2\right)^{-m-2+\frac{s-1}{\gamma-1}}\lambda_1^{2m-2+s}\mathrm{d}\lambda_1=\frac{x}{d} \tag{A.39}$$

where $s = 0$ or 1. According to the wall co-ordinates near the nozzle throat, it is implied that:

$$\frac{R}{d}=\frac{\sqrt{1-\frac{1}{4}\left[\frac{\mathrm{d}(r_{\mathrm{w}}/r_{\mathrm{nt}})}{\mathrm{d}(x/d)}\right]^2}}{\frac{1}{2}\frac{\mathrm{d}^2(r_{\mathrm{w}}/r_{\mathrm{nt}})}{\mathrm{d}(x/d)^2}} \tag{A.40}$$

Additionally, to take the derivative of λ to eq. (A.10), we get:

$$\frac{\mathrm{d}\lambda}{\mathrm{d}\frac{x}{d}}=\frac{1}{m}\left(\frac{\gamma+1}{2}\right)^{m-\frac{s}{\gamma-1}}\left(1-\frac{\gamma-1}{\gamma+1}\lambda_1^2\right)^{(m+2)-\frac{s-1}{\gamma-1}}\lambda_1^{-(2m-2+s)} \tag{A.41}$$

At the nozzle throat, according to eqs. (A.9), (A.11), and (A.12):

$$\frac{1}{m}=\sqrt{\frac{2d}{R}\left(\frac{\gamma+1}{2}\right)^{\frac{3\gamma-1}{\gamma-1}}} \tag{A.42}$$

The expression of eq. (A.13) is the same as that of Ishibashi and Takamoto [17]. It is obvious that the values of parameter m for both planar and axisymmetric nozzle flows are the same. If $R = 2d$, when $\gamma = 1.33$, 1.40, and 1.67, $m = 0.4997$, 0.4823, and 0.4219 respectively.

References

[1] Yin Z. Q., *et al.*, Discharge Coefficient of Small Sonic Nozzles, *Thermal Science*, *18* (2014), 5, pp. 1505-1510
[2] *** ISO 9300, Measurement of Gas Flow by Means of Critical Flow Venturi Nozzles, British Standard, October 21, 2005
[3] Wright, J. D., *et al.*, Thermal Effects on Critical Flow Venturis, *Proceedings*, 9th ISSFM, Arlington, Virg., USA, 2015
[4] Unsal, B., *et al.*, Numerical Assessment of Discharge Coefficient and Wall Temperature Dependence of Discharge Coefficient for Critical-Flow Venturi Nozzles, *Proceedings*, 9th ISSFM, Arlington, Virg., USA, 2015
[5] Bignell, N., Choi, Y. M., Thermal Effects in Small Sonic Nozzles, *Flow Measurement and Instrumentation*, *13* (2002), 1, pp.7-22
[6] Li, C. H., Mickam, B., Flow Characteristics and Entrance Length Effect for MEMS Nozzles, *Flow Measurement and Instrumentation*, *33* (2013), Oct., pp. 212-217
[7] Hu, C. C., *et al.*, Discharge Characteristics of Small Sonic Nozzles in the Shape of Pyramidal Convergent and Conical Divergent, *Flow Measurement and Instrumentation*, *25* (2012), June, pp. 26-31
[8] Illingworth, C. R., The Laminar Boundary-layer Associated with Retarded Flow of a Compressible Fluid, ARC RM 2590, 1946
[9] Li, T. Y., Nagamatsu, H. T., Similar Solutions of Compressible Boundary-Layer Equations, *Journal of the Aeronautical Sciences*, *20* (1955), 9, pp. 607-617
[10] Cohen, C. B., Reshotko, E., The Compressible Laminar Boundary-layer with Heat Transfer and Arbitrary Pressure Gradient, NACA Report 1294, Washington DC, 1956
[11] Ball, K. O. W., Similarity Solutions for the Compressible laminar Boundary-layer with Heat and Mass Transfer, *Physics of Fluids*, *10* (1967), 8, pp. 1823-1826
[12] Back, L. H., Acceleration and Cooling Effects in Laminar Boundary-layers-Subsonic, Transonic, and Supersonic Speeds, *AIAA Journal*, *8* (1970), 4, pp. 794-802
[13] Aziz, A., A Similarity Solution for Laminar Thermal Boundary-layer over a Flat Plate with a Convective Surface Boundary Condition, *Communications in Nonlinear Science and Numerical Simulation*, *14* (2009), 4, pp. 1064-1068
[14] Kendoush, A. A., Theoretical Analysis of Heat and Mass Transfer to Fluids Flowing Across a Flat Plate, *International Journal of Thermal Sciences*, *48* (2009), 1, pp. 188-194

[15] Tang, S. P., Theoretical Determination of the Discharge Coefficients of Axisymmetric Nozzles under Critical Flows, *Project SQUID Technical Report*, PR-118-PU, 1969
[16] Geropp, D., Laminar Boundary-Layers in Flat and Rotation-Symmetric Laval Nozzle (in German), *Deutsche Luft- und Raumfahrt Forschungsbericht*, 1971, pp. 71-90
[17] Ishibashi, M., Takamoto, M., Theoretical Discharge Coefficient of a Critical Circular-Arc Nozzle with Laminar boundary-layer and Its Verification by Measurements using Super-Accurate Nozzles, *Flow Measurement and Instrumentation*, *11* (2000), 4, pp. 305-313
[18] Johnson, A. N., *et al.*, Numerical Characterization of the Discharge Coefficient in Critical Nozzles, *Proceedings,* NCSL Workshop and Symposium, Albuquerque, N. Mex., USA, 1998, pp. 407-422
[19] Teodorescu, P. P., *Introduction to Thermoelectricity*, *Treatise on Classical Elasticity,* Springer, Amsterdam, The Netherlands, 2013, pp. 671-698
[20] Thomas, B. G., *et al.*, Analysis of Thermal and Mechanical Behaviour of Copper Molds During Continuous Casting of Steel Slabs, *Iron and Steelmaker*, *25* (1998), 10, pp. 125-143
[21] Park, J. K., *et al.*, Analysis of Thermal and Mechanical Behaviour of Copper Mould During Thin Slab Casting, *Proceedings,* 83rd Steelmaking Conference, Pittsburgh, Penn., 2000, Vol. 83, pp. 9-22
[22] Cragun, R., Howell, L. L., A Constrained Thermal Expansion Micro-Actuator, *Micro - Electro - Mechanical Systems* (MEMS), *66*, (1998), pp. 365-371
[23] Isfahani, A. H. G., *et al*., Simulating Thermal Stresses and Cooling Deformations, *Die Casting Engineer*, (2012), Mar., pp. 34-36
[24] Ansola, R., *et al.*, Evolutionary Optimization of Compliant Mechanisms Subjected to Non-Uniform Thermal Effects, *Finite Elements in Analysis and Design*, *57* (2012), Sept., pp. 1-14
[25] Stavely, R. L., Design of Contact-Aided Compliant Cellular Mechanisms for Use as Passive Variable Thermal Conductivity Structures, Ph. D. thesis, The Pennsylvania State University, Pittsburgh, Penn., USA, 2013
[26] Schlichting, H., *et al*., *Boundary-layer theory*, 8th ed., Springer, New York, USA, 2000
[27] Johnson, A., Numerical Characterization of the Discharge Coefficient in Critical Nozzles, Ph. D. thesis, The Pennsylvania State University, Pittsburgh, Penn., USA, 2000
[28] Hall, I. M., Transonic Flow in Two-Dimensional and Axially-Symmetric Nozzles, *Quarterly Journal of Mechanics and Applied Mathematics*, *15* (1962), 4, pp. 487-508
[29] Wang, C., *et al.*. Influence of Wall Roughness on Discharge Coefficient of Sonic Nozzles, *Flow Measurement and Instrumentation*, *35* (2014), Mar., pp. 52-62
[30] *** Fluent Inc., *Fluent User's Guide,* Fluent Inc.; 2003
[31] Versteeg, H. K., *et al*., *An Introduction to Computational Fluid Dynamics: the Finite Volume Method*, Wiley Press, New York, USA, 1995
[32] Sridhar, M. R., *et al*., Review of Elastic and Plastic Contact Conductance Models-Comparison with Experiment, *Journal of Thermophysics and Heat Transfer*, *8* (1994), 4, pp. 633-640
[33] Ding, H. B., *et al.*, An Analytical Method for Wilson Point in Nozzle Flow with Homogeneous Nucleating, *International Journal of Heat and Mass Transfer*, *73* (2014), June, pp. 586-594

Paper submitted: November 4, 2015
Paper revised: June 14, 2016
Paper accepted: June 23, 2016